

Iron-Bound Deadeyes from the Nineteenth-Century Akko Tower Wreck, Israel: Metallurgical Investigation of the Manufacturing Technology

I. Voiculescu¹ · V. Geantă¹ · A. Stern² · D. Ashkenazi³ · M. Cohen⁴ · D. Cvikel⁴

Received: 29 December 2016/Revised: 23 February 2017/Accepted: 23 February 2017/Published online: 9 March 2017
© Springer Science+Business Media New York and ASM International 2017

Abstract The Akko Tower Wreck is the remains of a 25-m-long merchant brig, which sank in Akko harbour during the second quarter of the nineteenth century. During underwater excavations, three iron-strapped deadeyes were retrieved from the shipwreck. Metallurgical investigation revealed information related to the manufacturing technologies of the objects. The presence of equiaxed grains combined with elongated inclusions indicates that the strops were made from indirect-smelted wrought iron manufactured by hot-forging and joined by riveting and forge welding. The welding zone of the loop was identified as a plain lap joint, and that of the chain links as a scarf joint. The high concentration of inclusions found on the -forge-welding fracture surface may indicate the use of sand as the flux material. The composition, microstructure and manufacturing technology suggest that the deadeyes were manufactured during the second quarter of the nineteenth century, which supports the dating of the ship by other evidence.

Keywords Akko Tower Wreck · Archaeometallurgy · Deadeye · Forge welding · Microstructure · Riveting · Wrought iron

Introduction

The Akko Tower Wreck

The historic walled port city of Akko (Acre, St. Jean d’Acre, Akka) is located at the northern extremity of Haifa Bay, in northern Israel (Fig. 1). In 1966, during an underwater survey of the ancient harbour of Akko, a shipwreck designated as the Akko Tower Wreck was discovered. The shipwreck site is situated about 35 m north of the Tower of Flies, after which it was named (Fig. 1), at a maximum depth of 4.4 m. Since this discovery, it has been surveyed twice, in 1975 and 1981 [1, p. 222; 2, p. 195; 3]. However, the researchers came to conflicting conclusions regarding the original ship. Consequently, four seasons of underwater excavations were conducted in 2012, 2013, 2015 and 2016 by the Leon Recanati Institute for Maritime Studies of the University of Haifa.

The shipwreck, lying north-east to south-west, is 17.8 m long and 6.4 m wide. Among the hull remains were sections of the keel, rising wood, keelson, hull planks, framing timbers, ceiling planks, limber boards, and longitudinal reinforcing components [4]. Preliminary study of the shipwreck indicated that it is the remains of a 25-m-long merchant brig, dated to the first half of the nineteenth century, and built under the influence of the French shipbuilding tradition in an established shipyard [4, 5].

A variety of items was found during the excavations, comprising rigging elements, wooden and metal objects, ceramic floor tiles, and stones. The finds were documented

✉ D. Ashkenazi
dana@eng.tau.ac.il

¹ University Politehnica of Bucharest, 060042 Bucharest, Romania

² Department of Materials Engineering, Ben-Gurion University of the Negev, 8410501 Beer Sheva, Israel

³ School of Mechanical Engineering, Tel Aviv University, 6997801 Ramat Aviv, Israel

⁴ Department of Maritime Civilizations, Leon Recanati Institute for Maritime Studies, University of Haifa, 3498838 Haifa, Israel

Fig. 1 Location of Akko and the Akko Tower Wreck (Drawing: N. Yoselevich and J. Asuli)



on site, retrieved, registered, and are being studied [4]. Among the rigging elements were iron-strapped deadeyes—the subject of this article.

The Iron-Strapped Deadeyes

Important information can be derived from rigging elements about various aspects of the ship [6]. Deadeyes were components of the standing rigging of a ship and were used in pairs to secure the ends of shrouds to a chain plate fixed to the hull, in order to provide lateral support to the masts. The deadeye was a round, flat, hardwood block, pierced with three holes. Around its circumference was a flat groove for an iron strap, or a groove for a rope, depending on its use. A lanyard was reeved through the holes in each pair of deadeyes, allowing the shroud to be set up taut by

pulling them together [7, p. 11; 8, p. 410; 9, pp. 234–235; 10, pp. 168–169; 11, p. 251; 12, p. 165].

The shape of the deadeyes and their assemblage has changed through the centuries. Drop- or pear-shaped deadeyes were used from about the mid-fifteenth to the first half of the seventeenth century. From the middle of the seventeenth century, round deadeyes came into use [13, p. 70 figs. 49 and 50; 14, p. 244]. Ships of all nations used futtock plates, ‘a narrow plate of iron, having a deadeye bound in the upper end’ [7, pp. 13–14], during the first four decades of the seventeenth century. Later, round-section iron strops were used in Europe, but the British reverted to flat-section iron strops around the mid-seventeenth century and retained this design throughout the eighteenth century [13, p. 68].

During underwater excavations, two concretions were retrieved from the northern section of the wreck site

(Fig. 2). Radiographic tests (RT) were performed on the concretions before taking any action that might have damaged the archaeological find [15, p. 444], which was subsequently carefully disassembled by breaking the concretion coating. Three deadeyes were exposed: two deadeyes, 163A and 163B, were connected by their thick concretion layer. Deadeyes 163A and 164 were in a good state of preservation, while 163B was less well preserved. Each one comprised an iron strap which encircled the wooden block, a futtock plate, and a chain with 14 surviving links at the lower end (Fig. 3a, b). The chain, referred to as the ‘futtock shroud’ [9, p. 332; 10, p. 54], was connected to the futtock plate using a shackle closed with a bolt and pin [7, p. 27]. The presence of the iron strap and the chain indicate that the deadeyes functioned as the lower deadeyes of a pair, and were probably used for rigging the topmasts [8, p. 1214; 9, p. 332; 10, p. 54; 11, pp. 67–68].

The wooden deadeyes were made of oak (*Quercus* sp.) and had an average diameter of 15.5 cm and an average thickness of 9.5 cm. The overall length of the deadeye and the futtock plate was 58.3 cm. The length of deadeye 163B bolt was 6 cm, and its outer diameter was 32 mm. The diameters of deadeye 164 chain links 4 and 5 were 14.4 and 14.1 mm, respectively [5]. All the dimensions mentioned in this work are those of the archaeological items and not of the original manufactured objects.

Under the concretion layers, the artefacts suffered from corrosion on their surface, but their core was well preserved (Fig. 3). Deadeye 163A was the best preserved of the three. Previous XRF and SEM–EDS chemical analysis of the straps demonstrated that they were made of wrought iron containing small amounts of P, Si, Mn, S, Al, Ca, Mg, and Cu [5]. Metallographic observation of the straps revealed a ferrite matrix, with 50- to 80- μm equiaxed

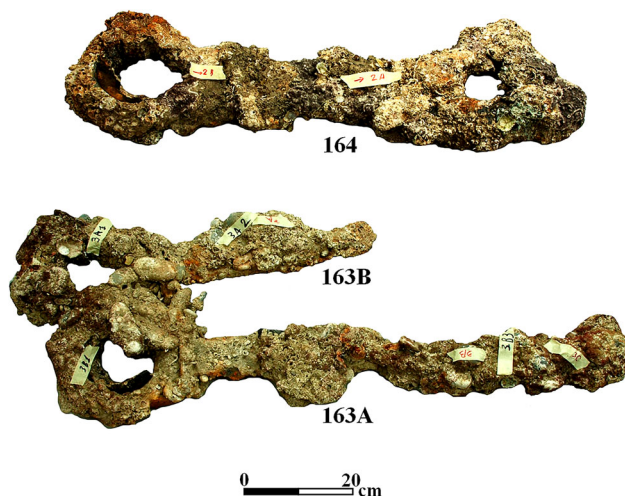


Fig. 2 Iron-bound deadeyes covered with a thick concretion coating (Photo: J. J. Gottlieb)

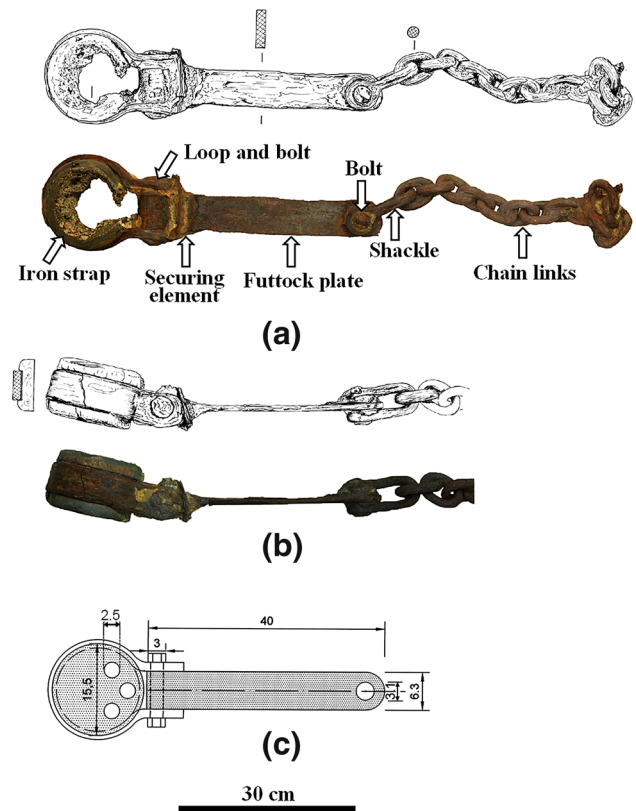


Fig. 3 Deadeye 163A: (a) top view of the deadeye, showing the loop, bolt and securing element; (b) side view of the deadeye (Photographs: J. J. Gottlieb, Drawing: R. Pollak); and (c) suggested reconstruction of the deadeye (Drawing: A. Ben Zeev)

grains (both at the L-CS and T-CS) and preferentially oriented slag inclusions at their L-CS [5].

The present study examined two main components: the futtock plate and the chains, and one secondary part—the bolt (rivet)—connecting the futtock plate to the iron strap. Two joining methods, common in the nineteenth century, were used to assemble the deadeyes: riveting and solid-state forge welding.

Metallurgical Background to Research

Wrought Iron

Ancient iron objects were produced by direct smelting (single-stage solid-state technology) of the ore called ‘bloomery’, which was carried out in a furnace at temperature below the melting point of iron and in a reducing atmosphere [16–19]. Until the middle of the nineteenth century, wrought iron products were manufactured by either the direct or the indirect smelting method [20]. In the direct bloomery smelting method (based on the Ellingham diagram), haematite (Fe_2O_3) was successively reduced to

magnetite (Fe_3O_4), wüstite (FeO) and then to iron metal [17, 18]. The bloom iron was a heterogeneous material containing a large amount of slag. Further hot-forging was required in order to remove the slag inclusions from the bloom and to transform the iron into a denser pig iron ingot suitable for further working [16, 18].

A variety of hearth furnaces for refining the pig iron were developed over the years. The most popular were the Catalan hearth furnaces, developed during the eighth century [21, 22]. The two-hearth process was invented later, and the most widely used hearths used the ‘Walloon’ forge method [23, p. 102]. The indirect smelting process of refining pig iron into malleable wrought iron, called the ‘puddling’ method, was developed by Cort in 1784 [23, pp. 128–129, 146, 166]. This innovation made it possible to increase wrought iron and steel production, satisfying the increasing demands of industry. The ‘puddling’ process permitted increasing wrought iron production capacity by using coal instead of charcoal and by avoiding contact between the metallic phase and fuel [24]. During the process, molten pig iron was exposed to gas burning at high temperatures, resulting in the oxidation of carbon. The stirring of molten pig iron, which was held separate from the charcoal fire in the furnace, exposed the metal uniformly to the elevated temperature of burning gas, oxidizing the carbon and reducing the iron oxide. This decreased the amount of carbon in the alloy, raising the melting temperature of the metal, and leading to formation of small pieces of semi-solid iron in the liquid material. Next the ‘puddler’ collected the small iron pieces and hammered them together into larger pieces [23, pp. 128–129, 146, 166].

The puddling technology was improved after 1816, when Hall implemented basic hearth lining. White cast iron covered with iron slag was inserted through charging doors into the heart of the furnace. The furnace doors were closed, and air was blown through the fire threshold zone to burn the coal until the melting temperature of the iron was reached. At this stage, it was possible to add more solid white cast iron. The hot metal was then removed from the furnace to be hammered and rolled, completing the conversion to workable wrought iron [23, pp. 128–129]. The common microstructure of indirect smelting wrought iron product consists of ferrite grains combined with slag inclusions embedded in the ferrite matrix. The inclusions are elongated, indicating the main direction of plastic deformation during the hammering [25, 26]. This technology of refining cast iron into wrought iron remained in common use until the middle of the nineteenth century [18].

Forge-Welding Principles and Practice

Until the end of the nineteenth century the usual joining methods for metal alloys were forge welding (FOW) and

riveting [23, pp. 174–175; [27–30]. FOW was used with great success in the production of steel tools, agrarian equipment, large structures, ships’ accessories and anchors [23, p. 174; 27, 28]. The main problem of FOW, when used in large structures, was the relatively high failure rate [23, p. 174; 25, 31]. At the end of the nineteenth century, several new joining techniques by melting of metal alloys were developed [32, 33, p. 3]. Since then, welding has been the most widely used method for joining metals.

The principles of the electric arc were first discovered by Davy in 1801. Nonetheless, it took another 80 years until the carbon–metal arc was used for electric welding [23, pp. 174–175; 30, 33, p. 3]. In 1887 Bernados registered a patent for carbon arc welding of steel, and after some changes the process became commercial about 1902 [23, p. 174].

Solid-State Welding

Solid-state welding (SSW) is a solid-phase joining method based on bringing the parts into such close contact that interatomic bonds are made [34]. When two metal surfaces are joined together under ideal conditions, the reduction in the energy caused by the elimination of the two free surface energies is usually enough to cause bonding between them [30, 34, 35]. However, joint formation does not take place under ideal conditions. In practice, the presence of adsorbed gases, oxide layers, rough surface topography, and other disturbances reduce the efficiency and quality of the contact even under high direct pressure. Therefore, these surface films must be removed before metallurgical bonding can be achieved. SSW methods, such as FOW, are effective at elevated temperatures when plastic flow helps to remove contamination layers [34].

Forge-Welding Process

FOW process is the oldest SSW technique used in various applications to bond similar or dissimilar ductile metals under pressure [23, pp. 42, 81]. When the process involves heating to a temperature below $0.3 T_m$ (T_m is the melting temperature in K), it is known as ‘warm welding’, and as ‘forge welding’ for temperatures above $0.3 T_m$. To achieve a metallurgical bond, atoms of one metal must be in contact with atoms of the other metal. A satisfactory FOW process should provide: (a) sufficient deformation so that surface films and contaminants are significantly removed, and/or (b) flux to help clean the surfaces to be joined [16, 36]. In FOW processes, creation of the intimate contact is done mechanically; that is, local yield stresses are exceeded on the contacting metal surfaces, and surface deformation is used to create the contact. Once the cleaned metal surfaces are in intimate contact, bonding can initiate [37,

pp. 286–287]. The bonding quality of clean metal surfaces depends on various factors, including lattice parameters, compatibility effects due to non-matching crystal structures, and/or crystallographic orientations at the interface [38]. The FOW bond strength depends significantly on the amount of plastic deformation, i.e., thickness reduction in the case of joining two metal surfaces. To initiate a bond between two contacting surfaces, the total deformation between the two gaps must exceed the so-called *threshold deformation*, below which the forge-weld zone would fracture after the removal of the applied load. As the deformation increases, the bond strength will increase until it reaches a maximum point called *optimal deformation* value, followed by a decrease in the joint strength [39, p. 227]. Both threshold deformation and optimal deformation values are material and process dependent; therefore, these values will alternate as the metal combinations and/or process parameters are changed.

In the nineteenth century, the necessary heat needed for the FOW process was obtained from a coal–gas and gas blowpipe. Normal practice was to apply flux to the interface to prevent re-oxidation of the surfaces to be joined [20, 36]. The typical FOW process consisted of dipping the hot workpieces in flux, and continuing heating until the iron parts had attained a cherry-red heat. The flux was then fused over the surfaces and dissolved any iron oxide which may have formed; the two surfaces were laid together and struck repeatedly, working towards the edges to expel the flux and assure a sound bonding of the workpiece [37, pp. 286–287; 40–43].

When two low-carbon steel parts are forge-welded, some of the residual oxides are typically entrapped along the weld [27, 44]. When heated further, the oxides spheroidize to minimize their surface energy. When alignments of round and/or elongated precipitates are observed along the joint, they may reveal the bond line of an older weld [16]. However, several heating/forging operations may result in homogenizing the matrix and deleting the bond line. Considering a FOW region between two ferritic layers of different compositions, the interface is typically characterized by a higher volume fraction of the non-metallic inclusions and by a finer grain size [36]. The detection of wüstite and fayalite (Fe_2SiO_4) phases in the microstructure will usually be one of the best ways to determine whether a workpiece has been produced from one lump or several [20, 27, 43, 44].

FOW is most commonly used on low-carbon steels at about 1100 °C, considerably below the melting temperature of iron [16, 44]. The steel parts can be used in the as-welded condition, but are usually subjected to a full annealing heat treatment after welding [44, 45]. One of the well-known applications of FOW was the production of iron shafts: forged shafts consisted in arranging a number

of iron slabs together, which were then heated and hammered into the required cylindrical form. When it became necessary to make longer shafts, this method was upgraded: an arrangement of slabs being taken as before, of which only a portion was welded and shaped to the circular form, a large piece of iron being left at one end, onto which more slabs could be forged as required [36, 44].

Experimental Methods and Testing

The wrought iron parts of the deadeyes were analysed by their typology and by applying metallurgical methods, using non-destructive testing (NDT) and destructive testing. The metallurgical examination was conducted on the loop of deadeye 163B and the chain links of deadeye 164 and included the following methods and parameters:

- (a) Visual testing (VT) of the deadeyes and their chain links in order to identify visible discontinuities.
- (b) Chemical analysis of the loop and chain link 2 was performed with a handheld XRF (HHXRF), equipped with a 45-kV Rh target x-ray tube. Light elements, including oxygen and carbon, could not be detected with this HHXRF, due to instrumental limitations. The area examined was 5 mm in diameter.
- (c) Optical emission spectroscopy (OES) analysis (with detection limit of <0.1%) was performed on the loop in order to examine the average carbon concentration. The area examined was 5 mm in diameter. The surface of the sample was cleaned prior to this test.
- (d) For the metallographic examinations of the loop (Fig. 4) and the chain links (Fig. 5), samples were cut in longitudinal (L-CS) and transverse (T-CS) sections according to ASTM E3-11 (2011) Standard and were mounted in Bakelite. The surface was roughly ground with 80 grit paper. It was then ground with 600–2500 silicon carbide grit papers, polished with 1- to 0.25- μm aluminium oxide polishing suspension and 0.1- μm synthetic diamond paste and then etched with Nital (97% alcohol, 3% HNO_3).
- (e) Light microscope (LM) examination of the objects was performed with an inverted system equipped with imaging analysis.
- (f) Scanning electron microscope (SEM) with EDS (energy-dispersive spectroscopy) analysis of the artefacts was performed (Tables 1, 2) with EDAX EDS in high vacuum mode with a secondary electron (SE) detector. Presence of less than 1 wt.% C could not be detected with this SEM–EDS, due to instrumental limitations.

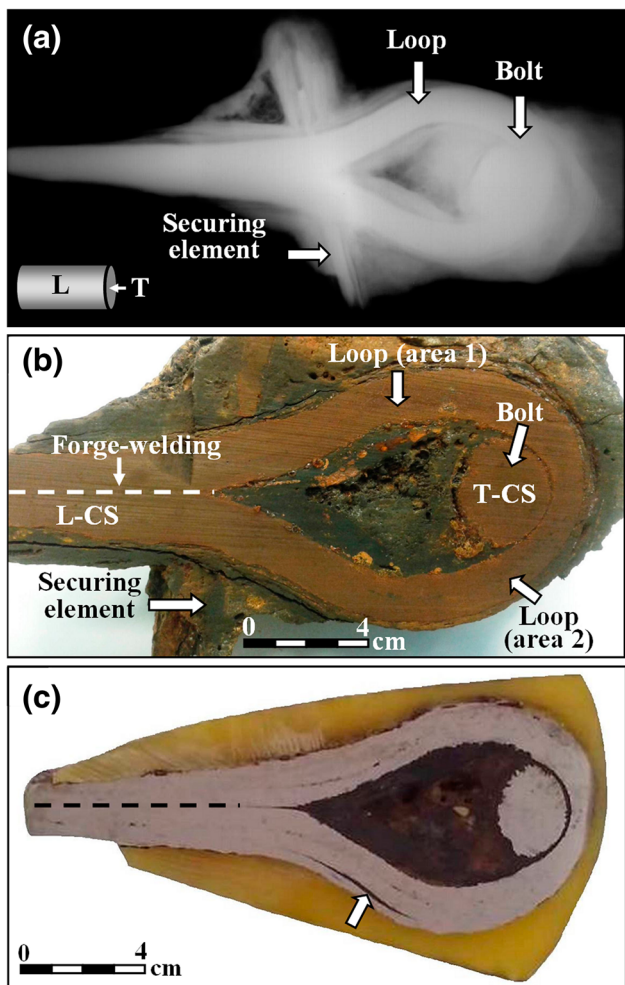


Fig. 4 Deadeye 163B loop: (a) radiographic image (Photo: A. Stern); (b) cross-section, showing the area of forge welding; and (c) cross-section after grinding and polishing, showing the hammering direction (arrow) and the forge-welding zone (dashed line) (Photo: I. Voiculescu)

- (g) Vickers microhardness measurements of the deadeye 163B loop and deadeye 164 bolt and chain links were performed with 200-gf load for 15 s (Table 3, after grinding and polishing of the artefact surfaces).
- (h) Fractography of notched specimens, broken by impact, was performed using a stereomicroscope, a digital image analysis system and SEM–EDS equipment. The subject will be elaborated in a future paper.

Engineering Description

Based on the VT and previous RT observation of deadeyes 163B and 164 [5], the objects (Figs. 3, 4, 5) were made of seven parts—five main components (the wooden deadeye, the circumferential iron strap, the futtock plate, the

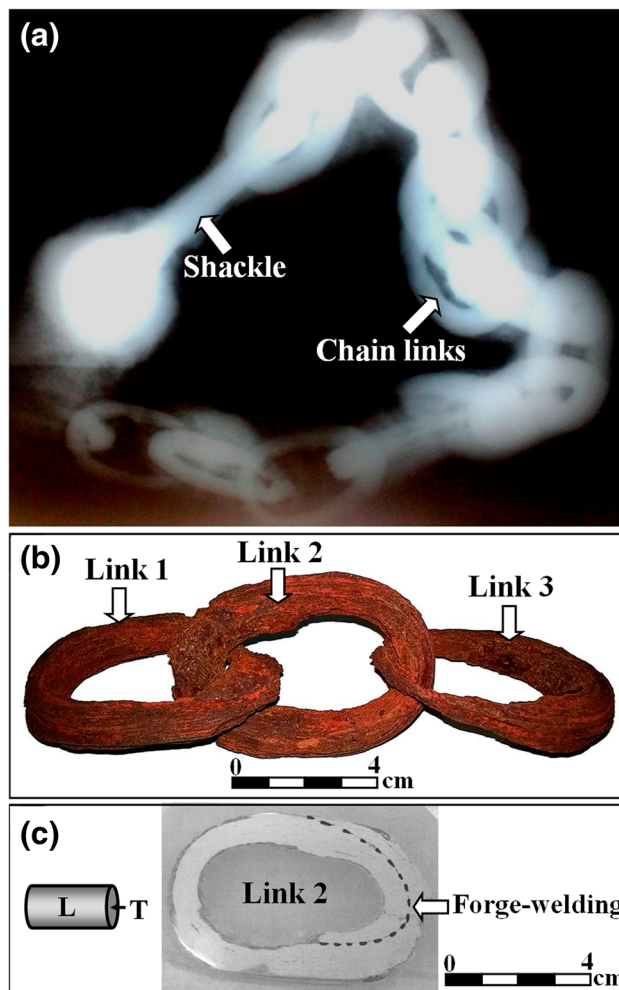


Fig. 5 Deadeye 164 chain links: (a) radiographic image of the shackle and chain links (Photo: A. Stern); (b) chain links 1, 2 and 3; and (c) cross-section of link 2 after grinding and polishing, showing the forge-welding zone (dashed line) (Photo: I. Voiculescu)

securing element, and the chain), and two secondary fasteners (the bolts serving as rivets and the shackle):

1. The deadeye—a round hardwood block, pierced with three holes.
2. The circumferential iron strap was attached and fitted to the deadeye (Fig. 3a). At both ends of the iron strap, suitable holes were drilled and a gap slightly larger than the futtock plate width was left open.
3. The futtock plate (Fig. 3a, b) was made from wrought iron, and a hole was drilled adjacent to one of the edges. The rectangular plate was then bent at the other edge, creating a closed loop joined by forge welding.
4. The bolt serving as a rivet (Fig. 4a, b) was cut from a hot-forged wrought iron rod.
5. The securing element (Fig. 4a, b) was made from a thin wrought iron plate.

Table 1 SEM-EDS chemical analysis of deadeye 163B loop and deadeye 164 chain link inclusions (local measurements of the polished metal away from the welding zone)

Measured area		Composition (wt.%)								
		Fe	O	Si	Mn	Mg	P	S	Al	Other elements
Deadeye 163B	Loop (L-CS, Fig. 6c, area 1)	83.1	13.0	1.1	0.5	–	2.3	–	–	
	Loop (L-CS, Fig. 6c, area 2)	73.6	18.0	2.6	1.0	–	2.8	–	1.2	0.5 Ti, 0.4 V
	Loop (L-CS, Fig. 6c, area 3)	59.4	21.7	8.9	1.8	–	6.4	0.9	0.7	0.1 Ti, 0.1 V
	Loop (L-CS, Fig. 6c, area 4)	64.6	18.5	7.9	1.3	–	5.3	1.7	0.5	0.1 Ti, 0.2 V
	Loop (T-CS, Fig. 6f, area 1)	57.5	20.6	7.1	1.6	–	10.4	1.0	1.3	0.3 Ti, 0.2 V
Deadeye 164	Chain link 2 (L-CS, Fig. 11e, area 2)	45.5	32.9	8.6	2.8	0.7	7.0	0.2	0.5	0.9 K
	Chain link 2 (L-CS, Fig. 11e, area 3)	47.9	31.9	8.5	2.6	0.5	5.9	1.2	0.3	0.1 K, 0.3 V
	Chain link 2 (L-CS, Fig. 11e, area 4)	48.9	31.5	9.8	2.9	0.7	5.4	0.2	0.4	–
	Chain link 2 (L-CS, Fig. 11e, average value of areas 1 and 5, base material)	99.6	0.2	–	–	–	0.3	–	–	–
	Chain link 2 (T-CS, Fig. 11g, area 1)	84.3	15.1	–	0.6	–	–	–	–	–
	Chain link 2 (T-CS, Fig. 11g, area 2)	77.6	17.0	2.7	0.9	–	1.9	–	–	–
	Chain link 2 (T-CS, Fig. 12g, area 3)	84.6	14.8	–	0.6	–	–	–	–	–
	Chain link 2 (T-CS, Fig. 11g, area 4, base material)	100.0	–	–	–	–	–	–	–	–

Table 2 SEM-EDS local area measurements of deadeye 163B loop forge-welding zone (after polishing)

Measured area		Composition (wt.%)									
		Fe	O	Si	Mn	Mg	P	S	Al	Ca	Other elements
FOW, L-CS (Fig. 9b, area 2)		78.3	21.7	–	–	–	–	–	–	–	–
FOW, L-CS (Fig. 9b, area 3)		43.0	31.8	11.1	–	–	3.4	1.7	3.2	5.2	0.6 K
FOW, L-CS (Fig. 9b, area 1, base material)		100.0	–	–	–	–	–	–	–	–	–
FOW, L-CS (Fig. 9d, area 1)		48.5	31.9	11.6	0.6	1.0	2.9	–	1.2	2.0	0.2 K
FOW, L-CS (Fig. 9e, area 3)		43.2	31.1	10.4	0.6	0.6	4.3	0.5	2.6	5.6	0.3 K, 1.0 Na
FOW, L-CS (Fig. 9e, area 4)		42.1	31.6	10.9	0.6	0.6	3.4	1.6	3.2	4.4	0.4 K, 1.2 Na
FOW, L-CS (Fig. 9e, area 5)		78.7	20.8	–	–	–	–	–	0.5	–	–
FOW, L-CS (Fig. 9e, area 6)		78.4	21.1	–	–	–	–	–	0.5	–	–
FOW, L-CS (Fig. 9e, average value of areas 1–4, base metal)		100.0	–	–	–	–	–	–	–	–	–
FOW, L-CS (Fig. 9f, area 2)		50.0	29.3	10.3	3.3	0.3	3.0	1.6	1.2	0.8	0.3 V
FOW, L-CS (Fig. 9f, area 3)		53.3	26.2	8.4	3.2	0.4	2.3	1.0	4.3	0.7	0.3 V
FOW, L-CS (Fig. 9f, area 4)		51.7	28.0	10.1	3.8	0.4	3.1	1.1	0.8	0.8	0.3 V
FOW, L-CS (Fig. 9f, area 5)		52.8	26.8	9.7	3.5	0.4	2.8	2.0	1.0	0.8	0.3 V
FOW, L-CS (Fig. 9f, average value of areas 1 and 6, base metal)		99.7	–	0.2	–	–	0.2	–	–	–	–

- The shackle (Fig. 3a) was made of wrought iron bar that was formed to its final shape by hot-forging.
- The chain—a wrought iron rod, was cut into short pieces to suitable dimensions (Figs. 3a, 5). Each piece was bent and forge-welded to make the chain links, and then the chain itself.

Metallurgical Analysis of the Loop and Chain Links

Deadeye 163B Loop

XRF analysis (average values) of deadeye 163B loop revealed composition of 98.1 wt.% Fe, 1.1 wt.% Si,

Table 3 Microhardness test (HV) of the iron artefacts

Sample		Vickers microhardness (HV)			
		Minimum	Maximum	Average	SD
Deadeye 163B, Loop	Away from weldment (L-CS)	137	144	141	2.8
	Near weldment (L-CS)	118	124	121	2.3
	Away from weldment (T-CS)	160	164	162	2.0
	Near weldment (T-CS)	165	170	168	2.1
Deadeye 163B, Bolt	Base metal (L-CS)	142	148	143	1.9
	Base metal (T-CS)	124	132	128	2.8
Chain link 2	Away from weldment (L-CS)	139	145	142	2.2
	Near weldment (L-CS)	166	169	167	1.1
	Away from weldment (T-CS)	149	150	150	0.5
	Near weldment (T-CS)	158	167	163	2.9

Ten measurements were made for each of the zones described in table. The distance of the indentation measurements from the weld line was approximately 100 µm

Fig. 6 Metallographic SEM images of deadeye 163B loop (no etching): **(a)** preferentially oriented slag inclusions (L-CS); **(b)** large preferentially oriented inclusion detected by the EDS analysis (arrow, L-CS); **(c)** higher magnification (×4000) of the large preferentially oriented inclusion; **(d)** and **(e)** slag inclusions (T-CS, LM); and **(f)** slag inclusions (dark areas) surrounded by iron ferrite matrix (T-CS, ×2000)

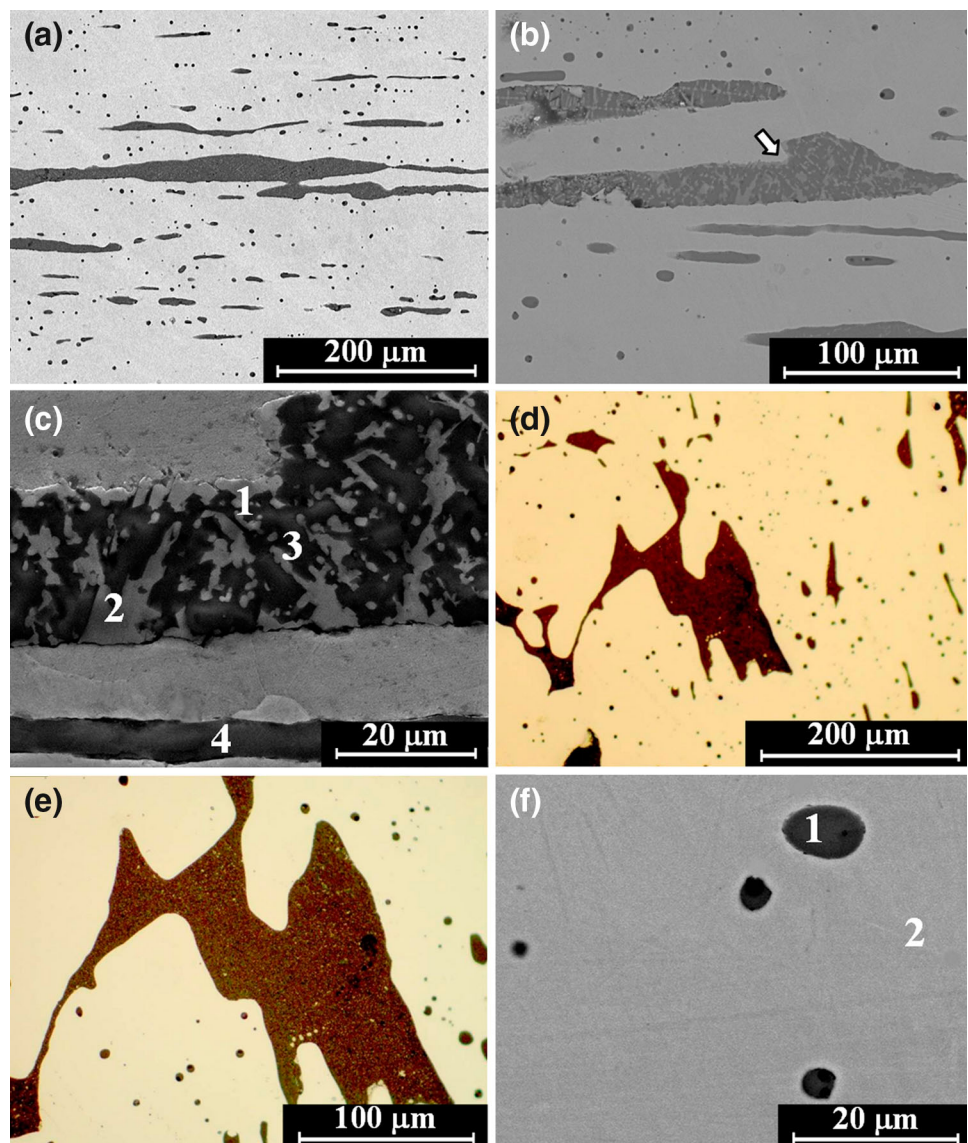
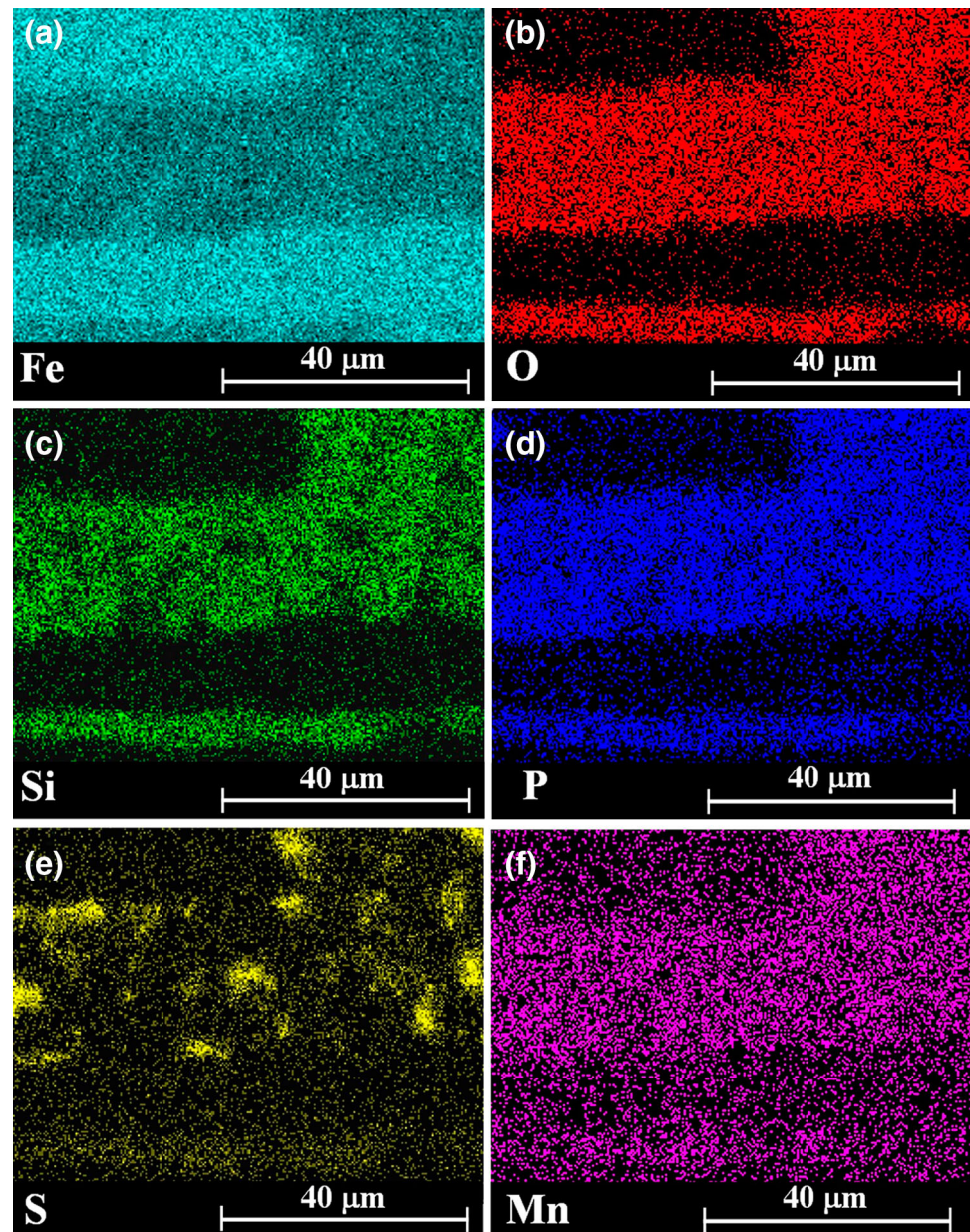


Fig. 7 Elemental analysis (SEM–EDS, bright dots) of the large preferentially oriented slag inclusion shown in Fig. 6c (deadeye 163B loop) showing the presence of the elements: (a) iron; (b) oxygen; (c) silicon; (d) phosphorus; (e) sulphur; and (f) manganese



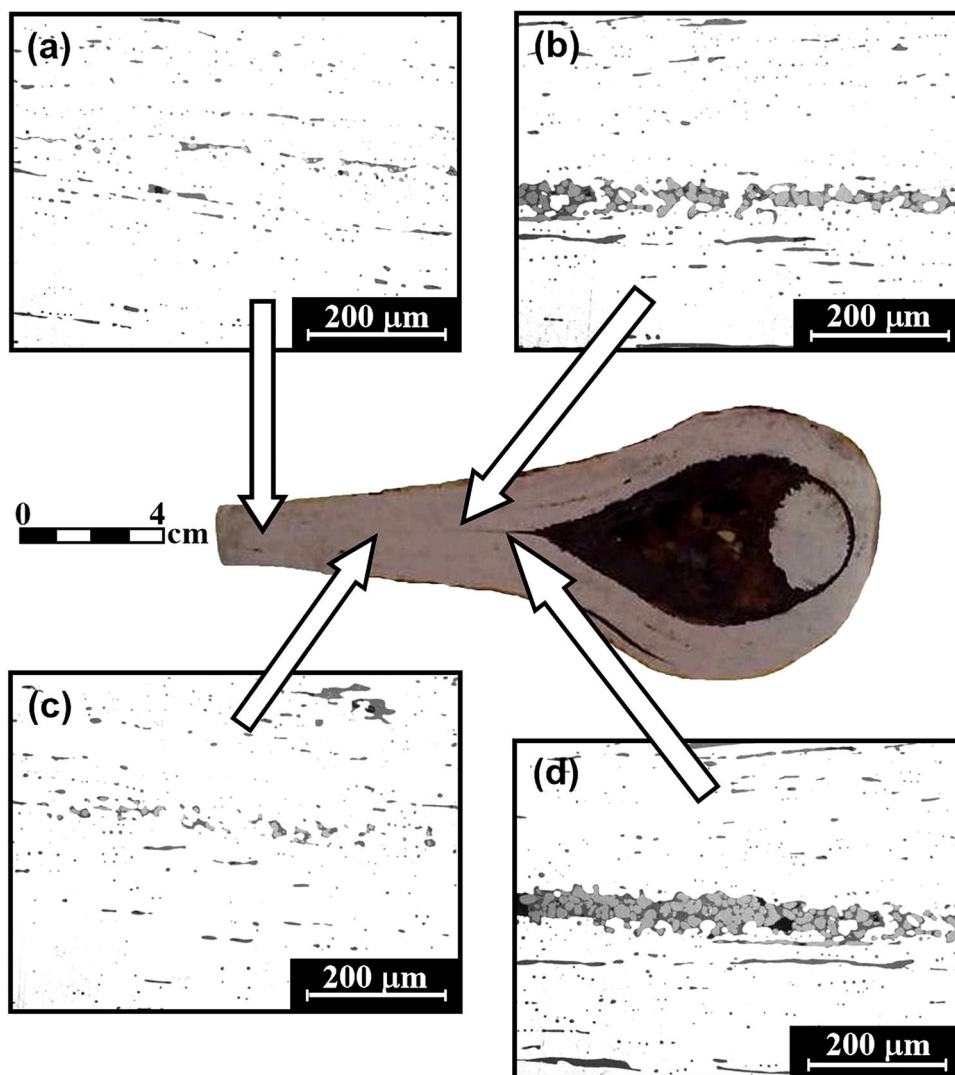
0.4 wt.% P, 0.2 wt.% S, 0.2 wt.% Al and 0.1 wt.% Mn. Chemical OES analysis of the loop indicated that it was made of iron containing 0.1 wt.% C. SEM–EDS analysis of the loop's iron matrix showed a composition of 99.3–100 wt.% Fe and up to 0.7 wt.% P.

The loop L-CS metallographic LM and SEM images showed a ferrite iron matrix containing elongated preferentially oriented slag inclusions (Fig. 6a–c), typical of hot-forged wrought iron. Metallographic images of the loop's T-CS revealed that the iron matrix contains slag particles having irregular or elliptical cross sections (Fig. 6d–f). The loop's iron matrix microhardness values ranged between

141 ± 2.8 HV at the L-CS and 162 ± 2.0 HV at the T-CS (Table 3).

The large elongated slag inclusion (Fig. 6b, c, points 1–3), according to the EDS local analysis, is composed of 59.4–83.1 wt.% Fe, 13.0–21.7 wt.% O, 1.1–8.9 Si wt.%, but also contains other elements, including Mn, P, S, Al, Ti and V (Table 1). The elemental area distribution of the same preferentially oriented two-phase slag inclusion also showed presence of Fe, O, Si, P, S and Mn (Fig. 7). The single-phase slag inclusion (Fig. 6f, area 1) is mostly composed of Fe (57.5 wt.%), O (20.6 wt.%) and Si (7.1 wt.%), but also contains minor quantities of Mn, P, S,

Fig. 8 Metallographic images of the forge-welding zones (deadeye 163B loop, L-CS, LM, $\times 200$): (a) good welding quality; (b) welding zone rich with inclusions, indicating the use of flux material; (c) good welding quality; and (d) welding zone rich with inclusions, indicating the use of flux material



Al, Ti and V (Table 1). Therefore, this single-phase slag inclusion is most likely a fayalite particle [25].

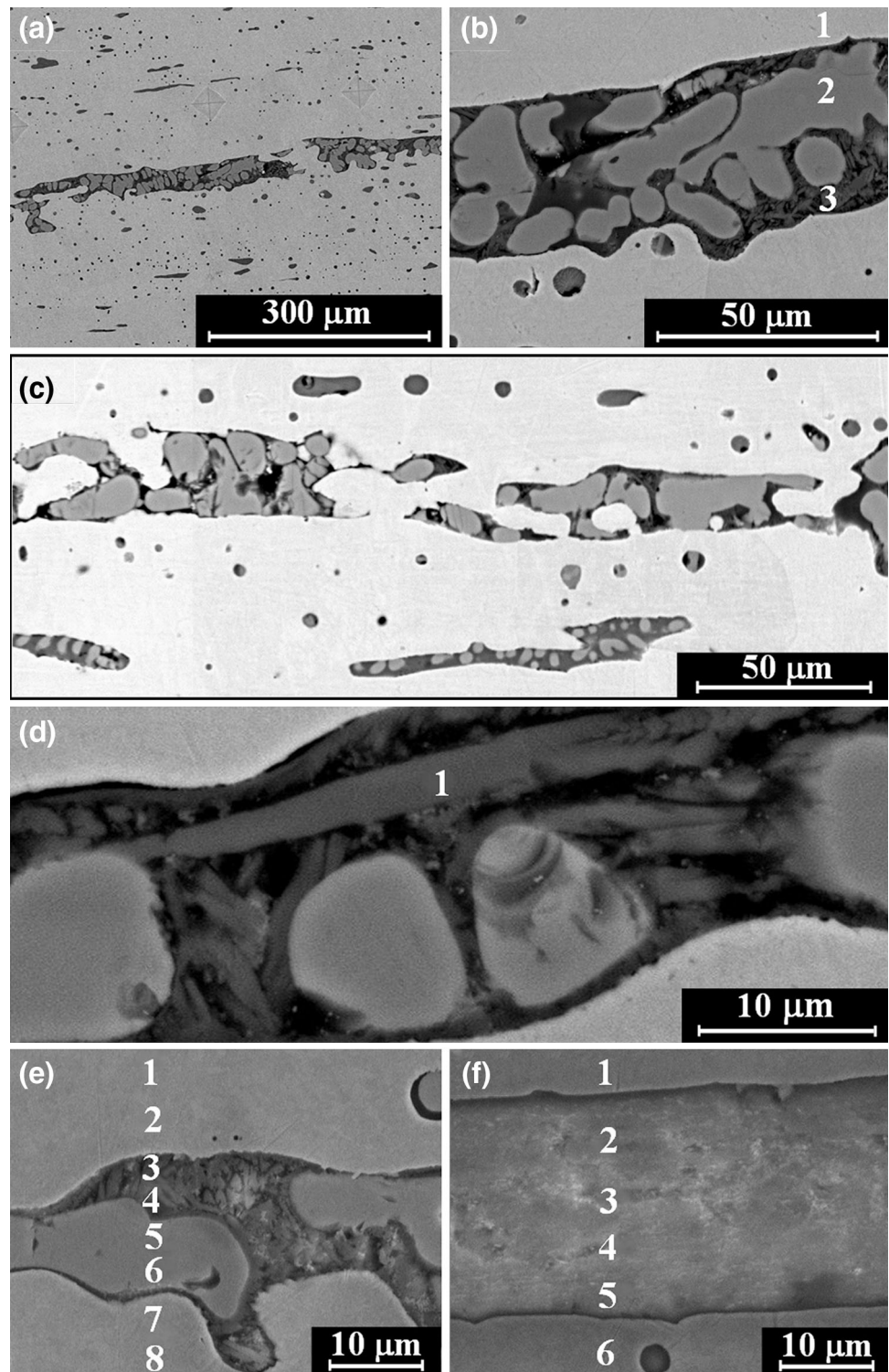
The Forge-Welding Zone of the Loop

Metallographic LM images of the loop's forge-welding zone revealed fragmented inclusions spread along the welding line (Fig. 8, L-CS). The loop's microhardness values near the forge-welding zone ranged from 121 ± 2.3 HV at the L-CS to 168 ± 2.1 HV at the T-CS (the \pm stands for the standard deviation, see Table 3).

SEM images of the loop's welding zone indicated the presence of two-phase and three-phase slag inclusions (Fig. 9, L-CS). According to the EDS analysis, the two-phase slag inclusion shown in Fig. 9b (areas 1 and 2) is composed of 43.0–78.0 wt.% Fe, 21.7–31.8 wt.% O and up to 11.1 wt.% Si, as well as S, Al, Ca, and K. Therefore, based on the composition and microstructure, this

slag inclusion is a wüstite–glass two-phase inclusion [25, 27]. The elongated particle inside the three-phase slag inclusion (Fig. 9d, area 1) contained 48.5 wt.% Fe, 31.9 wt.% O, 11.6 wt.% Si, as well as other elements, including Mn, Mg, P, S, Al, Ca and K. Therefore, the three-phase slag inclusion is a fayalite–wüstite–glass inclusion. The two-phase slag inclusion (Fig. 9e, areas 3–6) showed presence of 42.1–78.7 wt.% Fe, 20.8–31.6 wt.% O, and up to 10.8 wt.% Si, as well as other elements, including Mn, Mg, P, S, Al, Ca, K and Na. Therefore, based on its composition and microstructure, this is a wüstite–glass two-phase inclusion [25, 27]. The slag inclusion in Fig. 9f (areas 2–5) revealed presence of 50.0–53.3 wt.% Fe, 26.2–29.3 wt.% O and 8.4–10.3 wt.% Si, as well as other elements, including Mn, Mg, P, S, Al, Ca and V (Table 2). Therefore, this single-phase slag inclusion is most likely a fayalite particle [25].

Fig. 9 SEM metallographic images of the loop's forge-welding zone (deadeye 163B, L-CS, before etching): (a) general view; (b) the welding zone ($\times 3000$), showing points 1–3 examined by EDS analysis; (c) the welding zone surrounded by ferrite matrix and slag inclusions; (d) higher magnification of the welding zone, showing point 1 detected by EDS ($\times 6000$); (e) points 1–8 detected by EDS; and (f) points 1–6 detected by EDS



Deadeye 163B Bolt

The chemical composition of the deadeye 163B bolt was determined by XRF to be 98.5 wt.% Fe, 0.7 wt.% Si, 0.5 wt.% P and 0.2 wt.% Mn. OES analysis of the bolt

revealed that it was made of iron containing about 0.1 wt.% C.

LM metallographic images (L-CS) of the bolt's central zone demonstrated an iron matrix containing slag inclusions with a slight tendency for preferred orientation

Fig. 10 Metallographic images of deadeye 163B bolt: (a) large slag inclusions (dark areas) surrounded by ferrite matrix (LM, L-CS, etched); (b) iron matrix with slightly preferred oriented inclusions (L-CS, etched); (c, d) slag inclusions surrounded by ferrite matrix (T-CS, etched); (e) slag inclusions (dark areas) surrounded by ferrite matrix (L-CS, SEM, BSE mode, $\times 1000$); and (f) slag inclusions (T-CS, BSE)

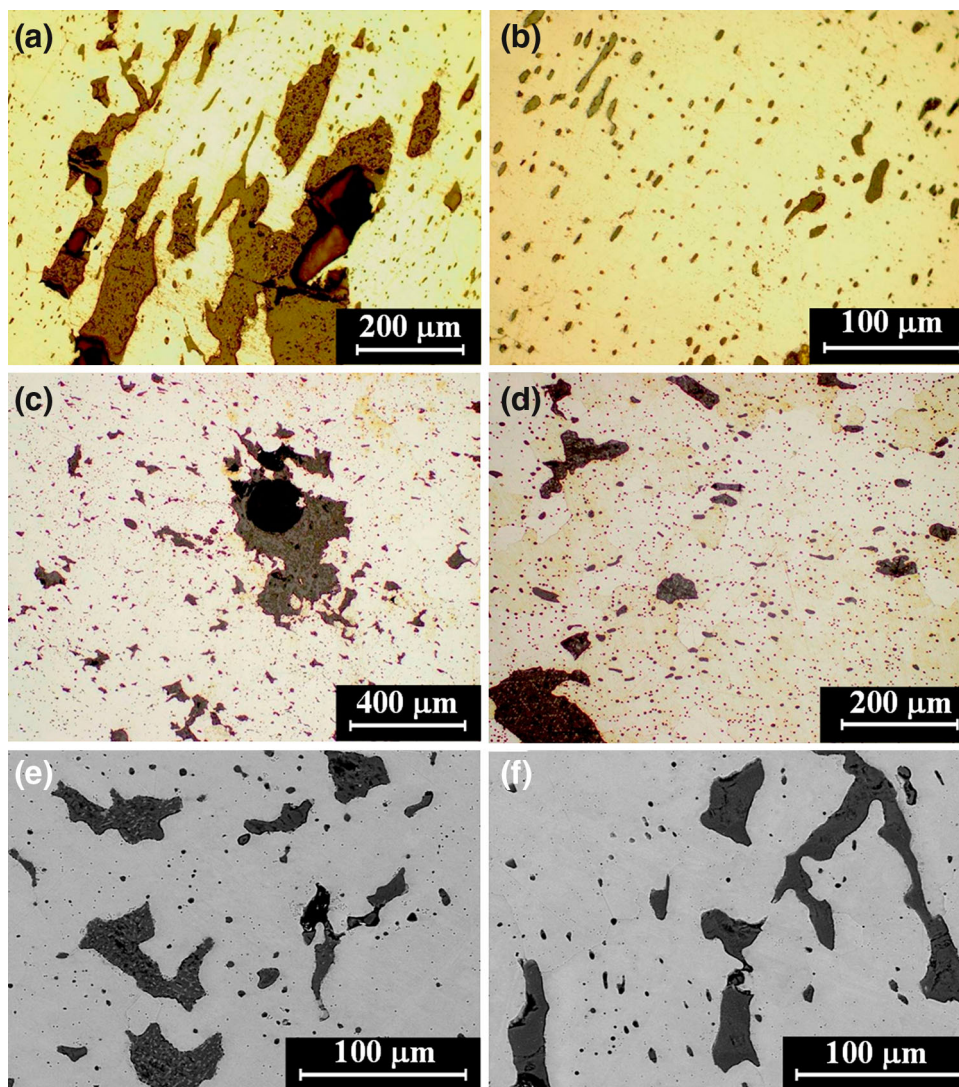


(Fig. 10). The bolt's iron matrix microhardness values ranged from 128 ± 2.8 HV at the T-CS to 142 ± 1.9 HV at the L-CS (Table 3).

Deadeye 164 Chain Links

Metallographic SEM–EDS analysis of chain link 2 L-CS (Fig. 11a–e) revealed that it was made of ferrite iron matrix, with composition of 99.4–99.7 wt.% Fe, up to 0.6 wt.% P and up to 0.3 wt.% O (Fig. 11e, near slag inclusion). Equiaxed ferrite grains, 50–100 μm in size, were observed after etching both the L-CS and T-CS samples (Fig. 11). The link's iron matrix microhardness values ranged from 142 ± 2.2 HV at the L-CS to 150 ± 0.5 HV at the T-CS, and the microhardness values near the welding zone ranged from 163 ± 2.9 HV at the T-CS to 167 ± 1.1 HV at the L-CS (Table 3).

The single-phase, two-phase and three-phase slag inclusions observed at the L-CS by LM and SEM were aligned in the direction of the hot-working process. The preferentially oriented slag inclusion shown in Fig. 11e (areas 2–4) is composed of 45.5–48.9 wt.% Fe, 31.5–32.9 wt.% O, 8.5–9.8 wt.% Si, 2.6–2.9 wt.% Mn and 5.4–7.0 wt.% P, with presence of other elements, including S, Al, K and V (EDS analysis, Table 1). Therefore, this single-phase slag inclusion is most likely a fayalite inclusion [20, 25].

SEM image of the link's T-CS indicated that it was made of iron (100 wt.% Fe, Fig. 11g, area 4, and Table 1) containing nearly circular slag inclusions surrounded by equiaxed ferrite grains (Fig. 11f, g, dark areas). The single-phase slag inclusion (Fig. 11g, T-CS, areas 1–3) is composed of 77.6–84.6 wt.% Fe, 14.8–17.0 wt.% O, and up to 2.7 wt.% Si, and also some Mn and P (Table 1). Therefore,

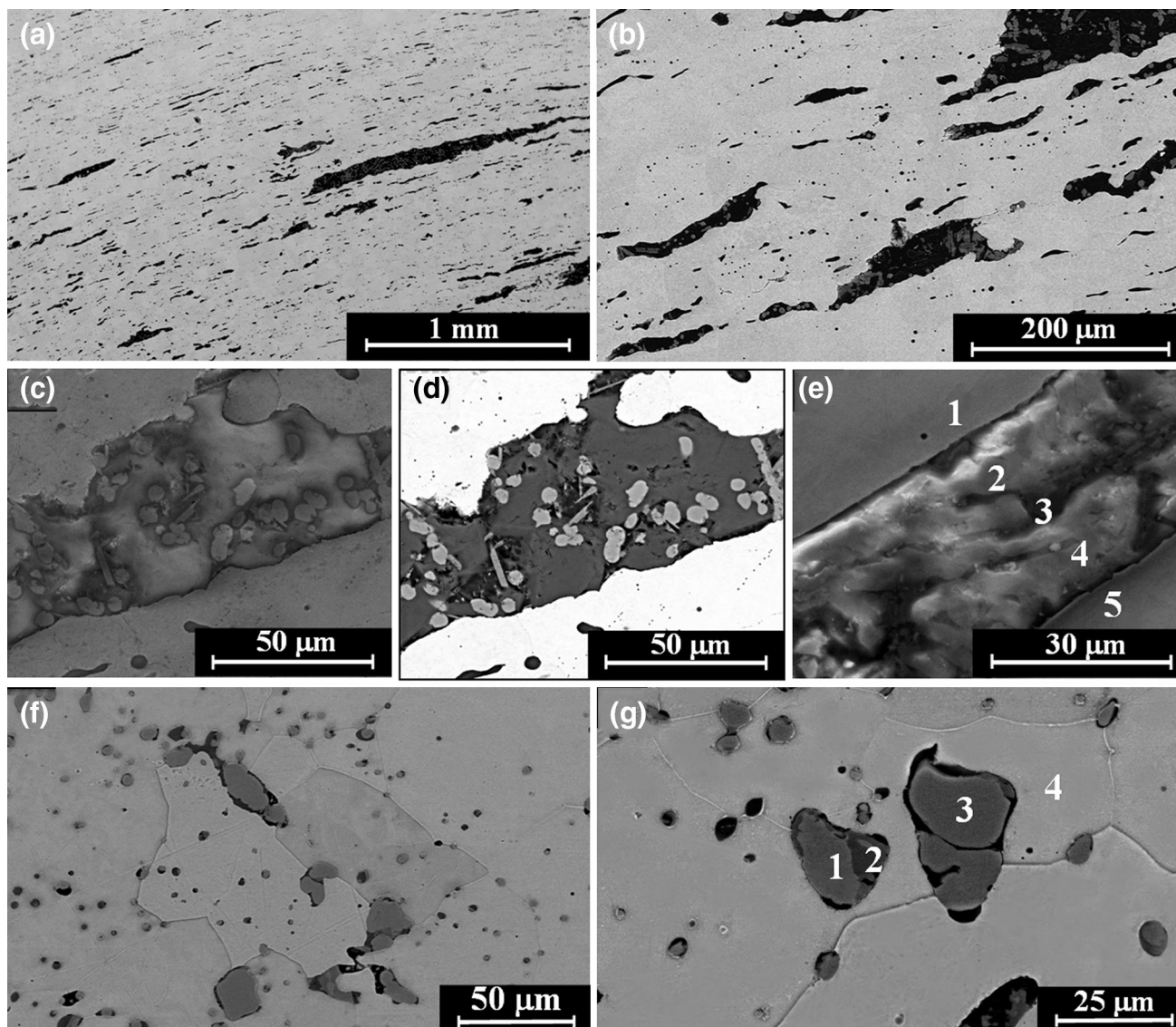


Fig. 11 Metallographic SEM images of chain link 2: (a) parallel preferentially oriented slag inclusions surrounded by ferrite matrix (L-CS, no etching); (b) higher magnification (L-CS, $\times 500$); (c) three-phase inclusion (L-CS, SE mode, $\times 2000$); (d) three-phase inclusion

this single-phase slag inclusion is most likely a fayalite inclusion.

The Fracture Surfaces

Deadeye 163B Loop (Base Material)

SEM examination of the loop's base material (far from the welding zone) revealed a complex fracture surface, composed of both ductile and brittle fracture surfaces, with presence of circular slag particles embedded in the iron matrix (Fig. 12). The ductile fracture surface exhibited dimples, known as microvoid coalescence topography

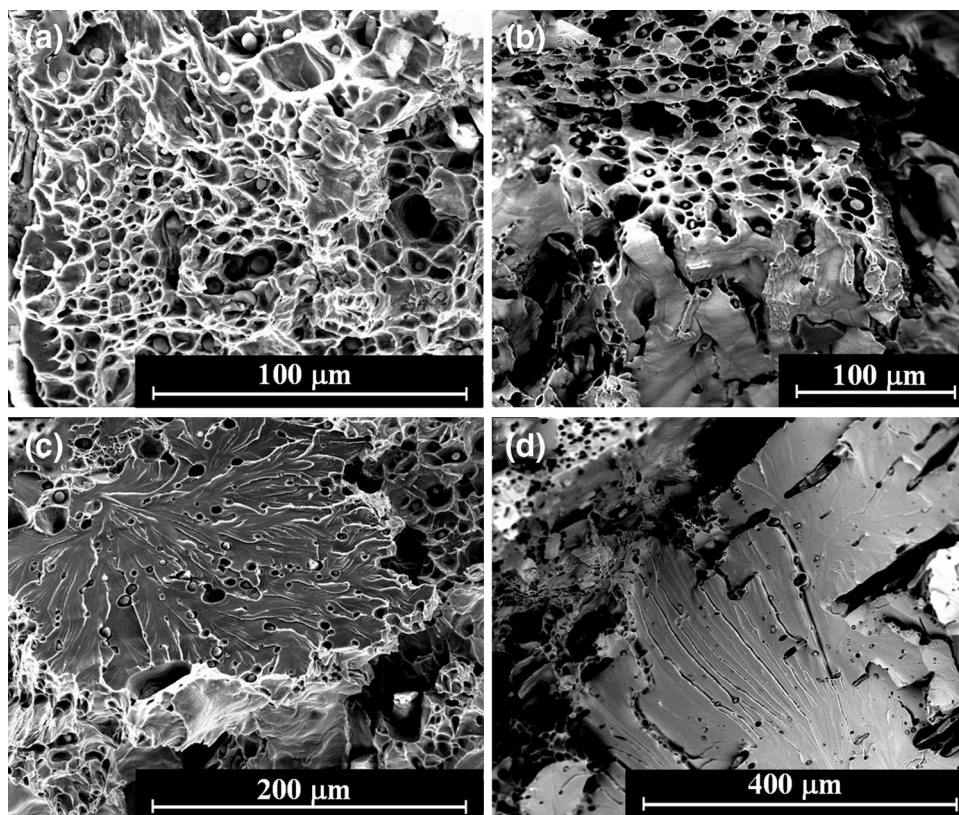
(BSE mode); (e) points 1–5 detected by the EDS (L-CS, SE, $\times 4000$); (f) ferrite matrix embedded with slag inclusions (T-CS, etched, SE, $\times 1000$); and (g) slag inclusions (dark areas 1–3) surrounded by ferrite matrix examined by EDS (T-CS, etched, $\times 2000$)

(Fig. 12a, b), and the brittle fracture surface includes 'river pattern' texture (Fig. 12c, d).

The Forge-Welding Zone of Deadeye 163B Loop

Ductile fracture surface, with dimpled microvoid coalescence topography, was observed at the forge-welding zone of deadeye 163B loop (Fig. 13a). The SEM-EDS elemental analyses of this fracture surface revealed the presence of the Fe, O, Si, P, S, Ca and Al (Fig. 13b–f). The EDS line scan of the fracture surface (Fig. 14a) indicates the presence of O, Si, P, S, Ca and Al in addition to iron. The relative intensity (III_0) indicates that the forge-welding zone consists of a ferrite matrix containing inclusion

Fig. 12 SEM images of the fracture surface of deadeye 163B, at the loop's base material: (a) ductile fracture with dimple structure (SE mode, $\times 2000$); (b) combination of ductile fracture (upper part of image) and brittle fracture (lower part of image) (BSE mode, $\times 1000$); (c) brittle fracture surrounded by ductile fracture (SE); and (d) brittle fracture surface of river pattern (BSE)



particles composed of Fe, O and Si, and of low quantities of P, S, Ca and Al (Fig. 14b). EDS area analysis of the fracture surface (scanned area of $250 \times 250 \mu\text{m}$) revealed composition of 82.0 wt.% Fe, 9.3 wt.% O, 2.5 wt.% C, 2.3 wt.% Si, 0.3 wt.% Mn, 0.7 wt.% P, 0.2 wt.% S, 1.1 wt.% Al, 0.3 wt.% Mg, 0.3 wt.% Na, 0.7 wt.% Ca, and less than 0.2 wt.% of K, Ni and Cl, typical of forge-welded wrought iron rich with slag inclusions and flux material residues.

Deadeye 164 Chain Link 2 (Base Material)

SEM observation of the fractured base material of chain link 2 exhibits a ductile morphology with a dimpled microvoid coalescence topography (Fig. 15a), but also areas with brittle fracture surface appearance displaying a ‘river pattern’ morphology (Fig. 15b). The observation of the fractured iron base metal also revealed presence of spherical single-phase particles embedded in the ferrite matrix for both ductile and brittle fracture surfaces (Fig. 15a, b, respectively). Such single-phase particles may be siliceous glassy inclusions, wüstite inclusions and/or fayalite inclusions.

The Forge-Welding Zone of Chain Link 2

SEM observation of the fracture surface at the forge-welding zone of chain link 2 exhibited ductile fracture

appearance with dimpled microvoid coalescence topography (Fig. 16a, b), combined with elongated inclusion particles (Fig. 16c), and spherical inclusion particles (Fig. 16d) embedded in the ferrite matrix.

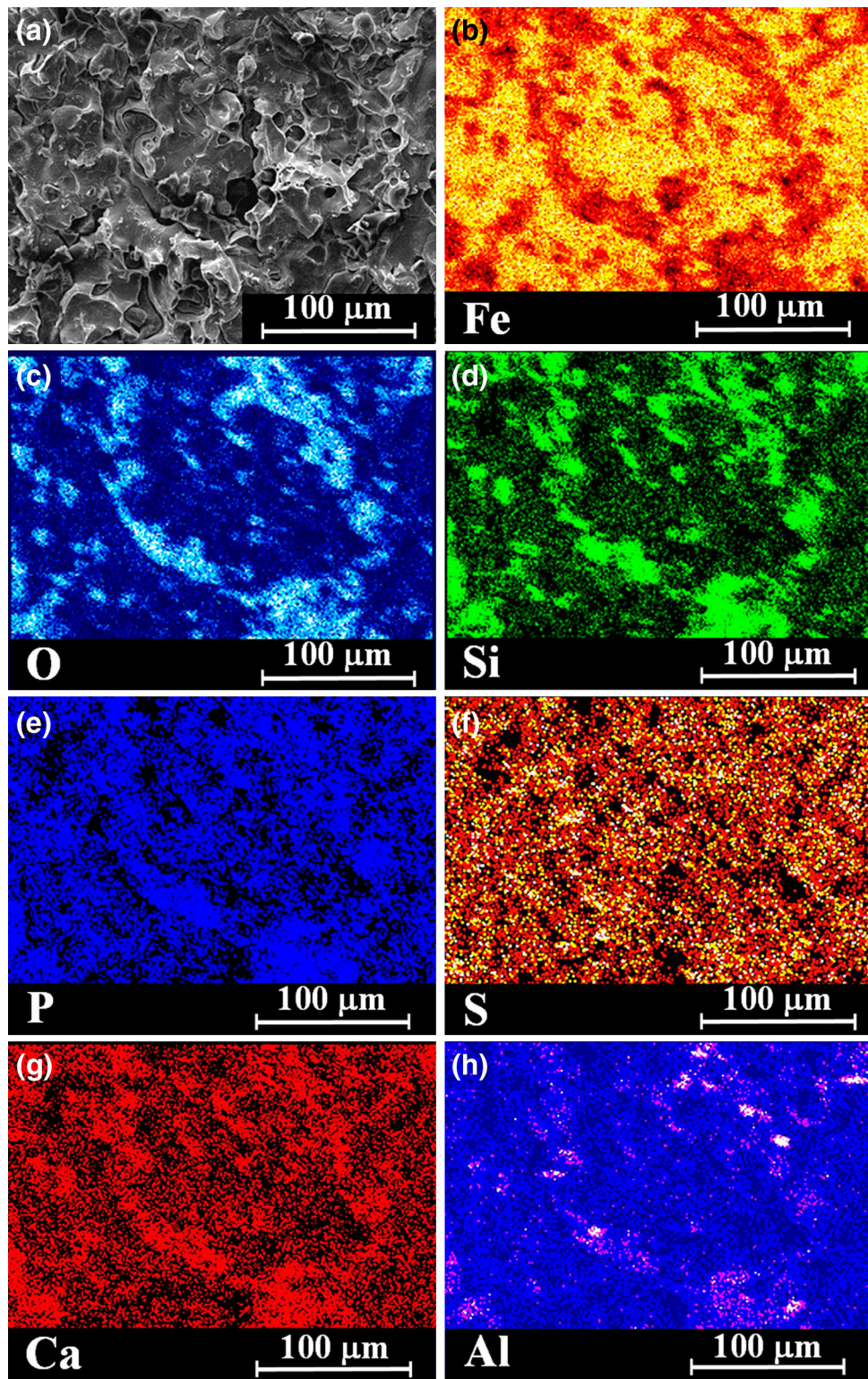
Discussion

Metallurgical Analysis of the Deadeyes

The metallurgical methodology used in this research contributed to understanding the manufacturing technology of the deadeyes, including the joining processes. The presence of ferrite equiaxed grains (with typical grain size of $50\text{--}100 \mu\text{m}$) combined with elongated slag inclusions (in the L-CS) indicate that the metal parts of the deadeyes were made of indirect wrought iron manufactured by the ‘puddling’ process, which was commonly used until the middle of the nineteenth century [20, 23, p. 146]. The deadeye parts had been shaped by hot-forging and joined by FOW and riveting processes.

According to the chemical OES analyses of deadeye 163B loop and bolt base material, both were fabricated of iron containing 0.1 wt.% C with relatively consistent carbon concentration, typical of wrought iron artefacts [18, 23, p. 48]. XRF analyses of the loop's base metal (average value) revealed that it was composed of iron containing

Fig. 13 Elemental analysis (SEM–EDS, bright dots) of the fracture surface of deadeye 163B loop, welding zone: (a) the fracture surface; (b) iron; (c) oxygen; (d) silicon; (e) phosphorus; (f) sulphur; (g) calcium; and (h) aluminium



1.1 wt.% Si, 0.4 wt.% P, 0.2 wt.% S, 0.2 wt.% Al and 0.1 wt.% Mn. XRF analysis of the bolt showed that it was composed of iron, with 0.7 wt.% Si, 0.5 wt.% P and 0.2 wt.% Mn. Si, Mn, P, S and Al are common in wrought iron slag inclusions [46]. Since Si does not reduce in either

direct or indirect smelting processes, its presence in the deadeye material represents the slag inclusions distributed in the wrought iron matrix [5, 18].

The morphology and orientation of the inclusions observed at the L-CS (LM and SEM) are indicative of the

Fig. 14 Line scan of deadeye 163B loop, fractured surface: (a) the scanned line (dashed white line); and (b) Intensity versus distance

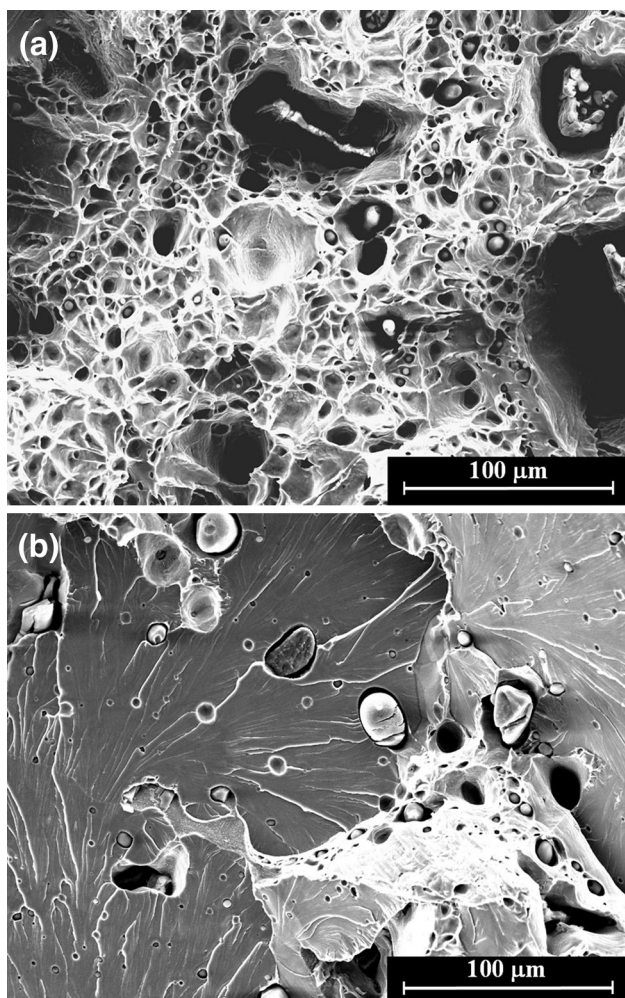
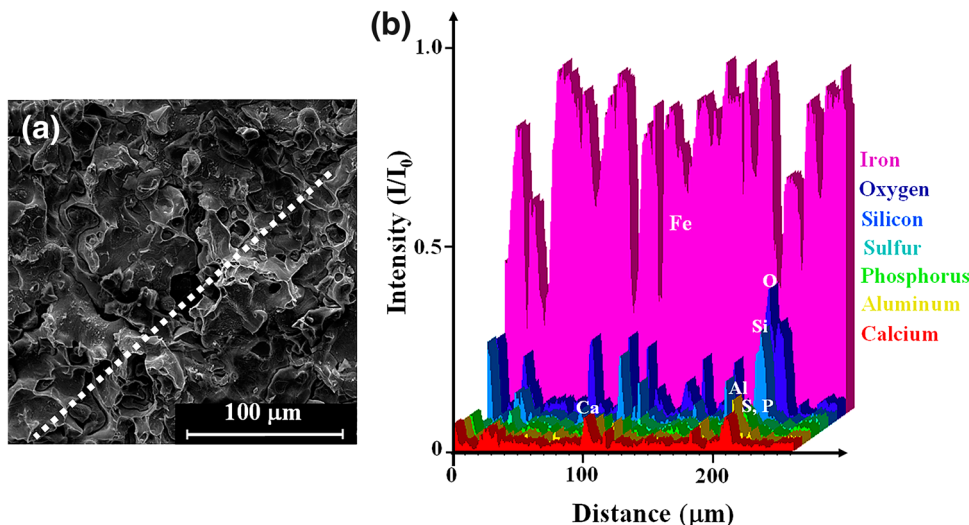


Fig. 15 SEM images (SE mode, ×1000 magnification) of the fractured surface at the base material of chain link 2: (a) typical ductile fracture of dimple structure; and (b) areas of brittle fracture surface (with river pattern) and ductile fracture surface (dimples at the lower part of image)

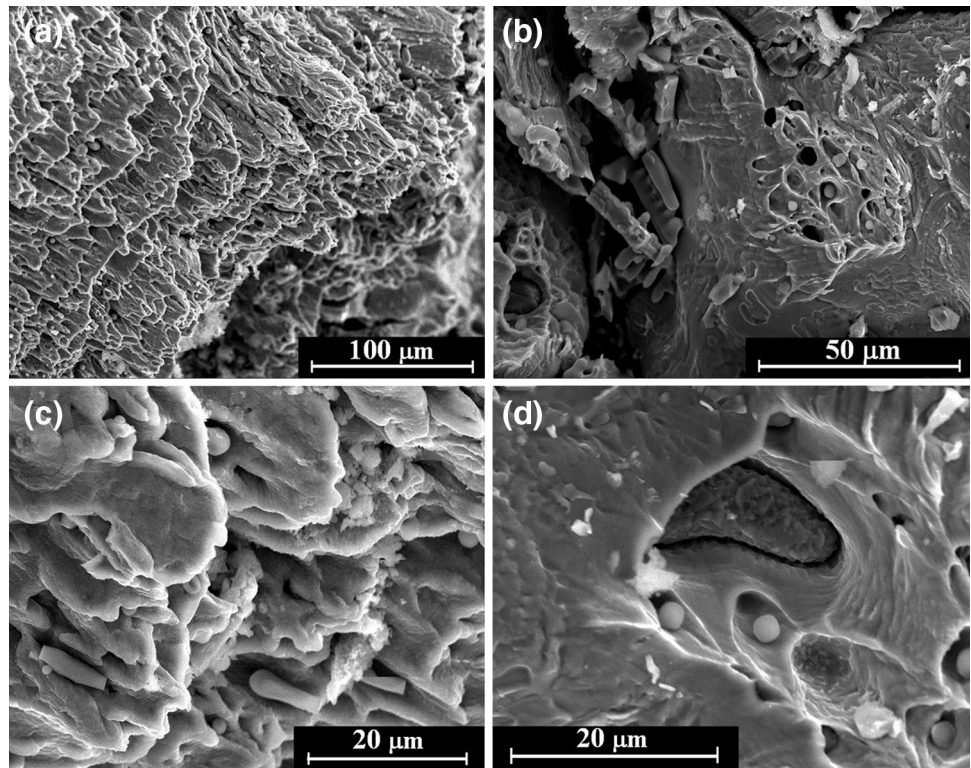
deformation during the hot-working process. Most of the inclusions had a large aspect ratio, indicating a significant deformation during the hot-forming of the loop (Fig. 6a–c).

The bolt’s L-CS microstructure shows that the slag inclusions are only slightly elongated and appear to be only partially preferred oriented (Fig. 10). The differences in composition and shape of the slag inclusions between the loop and the bolt indicate that they were most probably manufactured by different manufacturing processes.

EDS analysis of the chain link matrix demonstrated that it was composed of iron, with up to 0.6 wt.% P and up to 0.3 wt.% O. Examination of the link’s L-CS microstructure revealed that the appearance of the inclusions (Fig. 11a–e) is similar to the inclusion morphology observed in deadeye 163B loop; most inclusions are elongated (L-CS), indicating significant deformation during the manufacturing process.

Various slag inclusions were observed by SEM–EDS analyses in the base metal of the components (loop, bolt and chain link), including single-phase glassy slag inclusions; single-phase wüstite slag inclusions; single-phase fayalite slag inclusions; two-phase glass–wüstite inclusions; and three-phase glass–wüstite–fayalite slag inclusions; as well as iron phosphates and manganese sulphides. The slag inclusions (Table 1) were mostly composed of Fe, O and Si, but also contained other elements, including Mn, Mg, P, S, Al, K, Ti and V, which are common in wrought iron slag inclusions [5, 20, 25, 27]. Judging by the slag inclusion composition, measured in deadeye 163B loop and deadeye 164 chain link (Table 1), no Ti was found, except in the chain link inclusions; deadeye 163B futtock plate may have been manufactured from a slightly different wrought iron alloy from the 164 chain links. The inclusion morphology depends on the sampling orientation. In the T-CS, perpendicular to the direction of hot-working, the

Fig. 16 SEM images of the fracture surface at the forge-welding zone of chain link 2: (a) general view of the ductile fracture surface with elongated dimples ($\times 1000$); (b) mostly ductile fracture surface ($\times 2500$); (c) elongated inclusion particles embedded in the iron matrix ($\times 2500$); and (d) spherical inclusions embedded in the iron matrix ($\times 5000$)



inclusions are either flattened or slightly rounded; in the L-CS, the inclusions are strongly elongated, having a large aspect ratio, and therefore parallel strings of inclusions were observed.

Metallographic LM observation of the loop forge-welding zone of deadeye 163B revealed fragmented inclusions dispersed along the welding line (Fig. 8), with a morphology quite different from that in the base material. In most areas the lack of large inclusions at the interface indicates good bonding (Fig. 8a, b), whereas in other locations, large inclusions were observed along the interface, indicating low quality bonding (Fig. 8c, d). SEM images of the loop's welding zone revealed presence of single-phase, two-phase and three-phase slag inclusions (Fig. 9). Based on the inclusion compositions (Table 2), and the microstructure along the forge-welding line, the single-phase inclusions are most likely fayalite; the two-phase inclusions contain wüstite–glass, and the three-phase inclusions are made of fayalite–wüstite–glass [20, 25, 27].

The average microhardness values of the loop's base metal ranged from 141 ± 2.8 to 162 ± 2.0 HV; the bolt's iron values ranged from 128 ± 2.8 to 142 ± 1.9 HV; and the link's iron values ranged from 142 ± 2.2 to 150 ± 0.5 HV (Table 3). However, the loop's microhardness values in the forge-welding zone ranged from 121 ± 2.3 to 168 ± 2.1 HV (Table 3). Since the carbon concentration in all three items is very low, measured microhardness values

are mainly associated with plastic deformation and chemical composition [20]. The plastic deformation of the chain link was produced by rotating the workpiece in different directions, leading to more consistent microhardness values.

SEM fractographic examination of deadeye 163B loop base metal showed evidence of a mixed mode of ductile and brittle failure: ductile microvoid coalescence topography (Figs. 12a, b) and brittle 'river pattern' texture (Fig. 12c, d). This mixed mode failure behaviour may result from the composite nature of the wrought iron prepared by the puddling technique. The shape and number of the inclusions determine the form and size of the dimples [47]. Both the ductile and brittle fracture surfaces exhibited spherical single-phase inclusion particles embedded in the ferrite matrix. Such single-phase particles may be siliceous glassy inclusions, wüstite inclusions and/or fayalite, probably resulting from the use of sand flux (Fig. 12). In the future, it is recommended to further examine the inclusions embedded in the fracture surfaces.

The deadeye parts were joined by forge welding. Both the welding zones of the deadeye 163B loop and deadeye 164 chain links were located. Spherical particles were observed by SEM in the fractured area of the forge-welding zone of both the loop and the link (Fig. 16). The presence of slag inclusions embedded in the forge-welding zones and the high concentration of spherical particles observed

at the fracture surface of the welding zone may indicate the use of sand as flux material [48]. The forge-welding zone of deadeye 163B loop was identified as a plain lap joint; and that of deadeye 164 chain links was located and identified as a scarf joint.

Manufacturing Process of Each Part

It is suggested, based on the metallurgical analysis, that deadeye 163B loop and bolt (Figs. 3, 4) and deadeye 164 chain links (Figs. 3, 5) were manufactured as follows:

1. The futtock plate, 40 cm long, 6.2 cm wide and 1.3 cm thick (part 3), was made of wrought iron manufactured by the indirect smelting method, based on its composition and microstructure. The rectangular plate of iron was produced by hot-forging, based on the equiaxed ferrite grains and the inclusion shape. At one edge of the futtock plate, a hole was drilled, to connect the plate to the shackle by a rivet. Next, the second edge of the plate was bent into a loop, to enable joining the futtock plate to the circumferential iron strap fitted around the deadeye. Then the two loop edges were forge-welded using a plain lap joint configuration (Figs. 3a, 4a, b).
2. The bolt, about 3.2 cm in diameter (part 4, Fig. 4a, b), was cut from a wrought iron rod manufactured by forging a material produced by the indirect smelting method. The bolt served as a rivet connecting the futtock plate to the deadeye strap by a permanent mechanical joint.
3. The chain links (part 7, Figs. 3a, 5) were made of wrought iron rods manufactured by the indirect smelting method. Elliptical iron rods, with an average diameter of 1.4 cm, were cut into short lengths, and each length was bent into an elongated ring (average: 7.3×5.1 cm). The free ends were joined by forge welding using a scarf joint configuration to create the chain links, and by connecting the individual links to create the required chain length (Figs. 3, 5).

Assembly of the Final Object

Each deadeye assemblage consisted of seven individual parts. Based on the examinations, deadeye 163B was assembled as follows (Figs. 3, 4):

- The circumferential iron strap was attached and fitted to the deadeye.
- The futtock plate was attached to the iron strap by riveting, creating a permanent mechanical joint. It is suggested that the rivets were first placed in a furnace

and usually heated to white heat; as the hotter the temperature the more plastic and easily deformed is the rivet. Next the glowing rivet was inserted into the hole to be riveted, and then the riveter (or sometimes two riveters) hammered the unformed head into a mushroom shape fitting tightly against the joint.

- The securing element was probably attached to the futtock plate before the chain was connected.
- Finally the chain was secured to the futtock plate by inserted a bolt (rivet) into the shackle holes through the futtock plate (Fig. 3). The permanent mechanical joint was executed by riveting as above.

Thus, the solid-state forge welding along with the riveting mechanical joining method was employed to assemble the deadeye components. The composition, microstructure and the manufacturing technology of the iron parts suggest that they were manufactured during the second quarter of the nineteenth century, which supports the dating of the ship.

Conclusions

The components of the deadeyes retrieved from the Akko Tower Wreck were made of malleable wrought iron manufactured by the puddling technique, and were assembled by riveting and forge-welding techniques. The forge-welding zone of deadeye 163B loop was identified as plain lap joint, and those of deadeye 164 chain links were located and identified as scarf joints.

The high concentration of spherical inclusions containing substantial silicon and oxygen embedded in the wrought iron matrix, and found in the fractured area of the forge-welding zone, suggests that fine sand was used as flux material. Considering the chemical analysis and microstructure of the iron components, the use of riveting and forge welding methods, and the history of technological developments, it is suggested that they were manufactured during the second quarter of the nineteenth century, which supports the dating of the ship.

Acknowledgements The underwater excavations (IAA excavation permits G-23/2012, G-78/2013, G-16/2015 and G-25/2016) and research of the Akko Tower Wreck are supported by the Israel Science Foundation (Grant No. 447/12), the Honor Frost Foundation, D. Shafir, a Sir Maurice Hatter Fellowship, and the Rector and Research Authority of the University of Haifa, to whom the authors are grateful. The authors are grateful to Y. Shoef, Gabi Shoef Ltd, for the RT assistance; to V. Marinescu from ICPE-CA Bucharest for his valuable SEM assistance; to J. Tresman for the English editing; and to the anonymous reviewers for their valuable comments and suggestions.

References

1. A. Flinder, E. Linder, E.T. Hall, Survey of the ancient harbour of Akko, 1964–1966, in *Studies in the Archaeology and History of Ancient Israel*, ed. by M. Heltzer, A. Segal, D. Kaufman (Haifa University Press, Haifa, 1992), pp. 199–225
2. A. Raban, A shipwreck from Napoleon's siege of Akko (1799), in *Western Galilee Antiquities*, ed. by M. Yedaya (Ministry of Defense, Tel Aviv (in Hebrew), 1986), pp. 195–208
3. J.R. Steffy, The Napoleonic wreck: a workshop in ship construction (Unpublished report) (1983)
4. D. Cvikel, The nineteenth-century Akko Tower Wreck, Israel: a summary of the first two excavation seasons. *Int. J. Naut. Archaeol.* **45**(2), 406–422 (2016)
5. M. Cohen, D. Ashkenazi, A. Stern, Y. Kahanov, D. Cvikel, Iron artefacts from the Akko Tower Wreck, Israel, and their contribution to the ship's characterization, *Archaeo. Anthro. Sci.*, Published online: 8 March 2016. doi: [10.1007/s12520-016-0320-5](https://doi.org/10.1007/s12520-016-0320-5) (2016)
6. D. Sanders, Knowing the ropes: the need to record ropes and rigging on wreck-sites and some techniques for doing so. *Int. J. Naut. Archaeol.* **39**(1), 2–26 (2010)
7. G. Biddlecombe, The Art of Rigging Containing an Explanation of Terms and Phrases, and the Progressive Method of Rigging Expressly Adapted for Sailing Ships. Charles Wilson, (London/Dover Publications, New York, 1848, reprinted 1990)
8. W. Falconer, An Universal Dictionary of the Marine, T. Cadell, London (1780, reprinted 1970)
9. P. Kemp, *Oxford Companion to Ships and the Sea* (Oxford University Press, London, 1976)
10. J. Lees, *The Mast and Rigging of English Ships of War 1625–1860* (Naval Institute Press, Annapolis, 2007)
11. K.H. Marquardt, *Eighteenth-Century Rig and Rigging* (Conway, London, 2003). (reprint)
12. D. Steel, *The Elements and Practice of Rigging and Seamanship* (D. Steel, London, 1794)
13. R.C. Anderson, *The Rigging of Ships: In the Days of the Spritsail Topmast, 1600–1720* (Dover Publications, New York, 2012). (reprint)
14. Z.W. Mondfeld, *Historic Ship Models* (Sterling Publishing, New York, 2005)
15. C. Pulak, The Padlocks, in *Serçe Limanı: An Eleventh-Century Shipwreck Volume 1. The Ship and Its Anchorage*, ed. by G.F. Bass, G.F. Matthews, J.R. Steffy (Crew and Passengers, College Station, TX, 2004), pp. 437–452
16. E. Blakelock, M. Martinon-Torres, H.A. Veldhuijzen, T. Young, Slag inclusions in iron objects and the quest for provenance: an experiment and a case study. *J. Archaeol. Sci.* **36**(8), 1745–1757 (2009)
17. M. Cavallini, Thermodynamics applied to iron smelting techniques. *Appl. Phys. A* **113**(4), 1049–1053 (2013)
18. J.L. Coze, Purification of iron and steels a continuous effort from 2000 BC to AD 2000. *Mater. Trans.* **41**(1), 219–232 (2000)
19. M.L. Wayman, Archaeometallurgical contributions to a better understanding of the past. *Mater. Charact.* **45**(4), 259–267 (2000)
20. V.F. Buchwald, H. Wivel, Slag analysis as a method for the characterization and provenancing of ancient iron objects. *Mater. Charact.* **40**(2), 73–96 (1998)
21. V. Geantă, R. Ștefănoiu, *The Engineering of Steel Production* (Bren, Bucharest, 2008)
22. E. Tomàs, The Catalan process for the direct production of malleable iron and its spread to Europe and the Americas. *Contrib. Sci.* **1**(2), 225–232 (1999)
23. R.F. Tylecote, *A History of Metallurgy*, 2nd edn. (The Metals Society, London, 1992)
24. P. Belford, Hot blast iron smelting in the early nineteenth century: a re-appraisal. *Hist. Metall.* **46**(1), 32–44 (2012)
25. D. Cvikel, D. Ashkenazi, A. Stern, Y. Kahanov, Characterization of a 12-pdr wrought-iron cannonball from the Akko I shipwreck. *Mater. Charact.* **83**, 198–211 (2013)
26. N. North, M. Owens, C. Pearson, Thermal stability of cast and wrought marine iron. *Stud. Conserv.* **21**(4), 192–197 (1976)
27. A. Aronson, D. Ashkenazi, O. Barkai, Y. Kahanov, Archaeometallurgical investigation of the iron anchor from the Tantura F shipwreck. *Mater. Charact.* **78**, 108–120 (2013)
28. M. Eliyahu, O. Barkai, Y. Goren, N. Eliaz, Y. Kahanov, D. Ashkenazi, The iron anchors from the Tantura F shipwreck: typological and metallurgical analyses. *J. Archaeol. Sci.* **38**(2), 233–245 (2011)
29. Q. Collette, S. Sire, W.J. Vermes, V.J. Mesler, I. Wouters, Experimental investigations on hot-driven structural rivets in historical French and Belgian wrought-iron structures. *Constr. Build. Mater.* **54**, 258–269 (2014)
30. P.T. Houldcroft, Welding process developments and future trends. *Mater. Des.* **7**(4), 162–169 (1986)
31. R.F. Tylecote, *The Solid Phase Welding of Metals* (Edward Arnold, London, 1968)
32. D. Ashkenazi, D. Cvikel, M. Holtzman, D. Bershadski, A. Stern, S. Klein Y. Kahanov, The Dor C shipwreck, Israel: metallurgical analysis and its contribution to the ship characterization. *Archaeo. Anthro. Sci.*, Published online: 10 October 2015. (2015). doi: [10.1007/s12520-015-0296-6](https://doi.org/10.1007/s12520-015-0296-6)
33. R.-F. Stanescu, A single pass butt-welded pipe finite element method computer simulation. Unpublished Ph.D. dissertation, Carleton University, Ottawa (2005)
34. H.J. McQueen, Pressure welding, solid state: role of hot deformation. *Can. Metall. Q.* **51**(3), 239–249 (2012)
35. Å. Öberg, N. Mårtensson, J.Å. Schweitz, Fundamental aspects of formation and stability of explosive welds. *Metall. Trans. A* **16**(5), 841–852 (1985)
36. D. Ashkenazi, D. Cvikel, A. Stern, A. Pasternak, O. Barkai, A. Aronson, K. Kahanov, Archaeometallurgical investigation of joining processes of metal objects from shipwrecks: three test cases. *Metallogr. Microstruct. Anal.* **3**(5), 349–362 (2014)
37. T. Lienert, T. Siewert, S. Babu, V. Acoff (eds.), *Welding Fundamentals and Processes, ASM Handbook*, vol. 6A (ASM International, OH, 2011)
38. A. Stern, V. Shribman, A. Ben-Artzy, M. Aizenshtein, Interface phenomena and bonding mechanism in magnetic pulse welding. *J. Mater. Eng. Perform.* **23**(10), 3449–3458 (2014)
39. S. Mahabunphachai, M. Koc, J. Ni. Characterization of pressure welding process of thin sheet metals in cold and warm temperature conditions. In *ASME 2007 International Manufacturing Science and Engineering Conference* (American Society of Mechanical Engineers, Atlanta, 2007), pp. 227–233
40. H.J. McQueen, Successful transition from wrought iron to steel in hot work processing with mechanism differences. *Mater. Sci. Forum* **638–642**, 3380–3387 (2010)
41. J.D. Light, Observations concerning the hand forging of wrought iron. *Mater. Charact.* **45**, 327–340 (2000)
42. H.A. Mohamed, J. Washburn, Mechanisms of solid state pressure welding. *Weld. J. Res. Suppl.* **54**, 302s–310s (1975)
43. A. Stern, D. Ashkenazi, D. Cvikel, B. Rosen, E. Galili, Archeometallurgical and technical characterization of seventh century AD iron fishing-spear and fire basket found in the Dor lagoon, Israel. *J. Archaeol. Sci. Rep.* **3**, 132–143 (2015)
44. N.C. Ciarlo, H. De Rosa, D. Elkin, H. Svoboda, C. Vázquez, D. Vainstub, L. Diaz, Perdiguero, examination of an 18th century English anchor from Puerto Deseado (Santa Cruz Province, Argentina). *Hist. Metall.* **45**(1), 71–79 (2011)

45. M. Giles, Making metal and forging relations: ironworking in the British iron age. *Oxf. J. Archaeol.* **26**(4), 395–413 (2007)
46. R.E.M. Hedges, C.J. Salter, Source determination of iron currency bars through analysis of the slag inclusions. *Archaeometry* **21**(2), 161–175 (1979)
47. L. Engel, H. Klingele, *An Atlas of Metal Damage, Surface Examination by Scanning Electron Microscope* (Wolfe Publishing, Arizona, 1981)
48. J.G. Adelantado, M.F. Ferrer, F.V. Algarra, J.P. Vicente, F.B. Reig, Analytical study by SEM/EDX and metallographic techniques of materials used in the iron production process during the Iberian period. *Talanta* **60**(5), 895–910 (2003)